Protein Folding

International Edition: DOI: 10.1002/anie.201508968
German Edition: DOI: 10.1002/ange.201508968

Microtubule-Binding R3 Fragment from Tau Self-Assembles into Giant Multistranded Amyloid Ribbons

Jozef Adamcik, Antoni Sánchez-Ferrer, Nadine Ait-Bouziad, Nicholas P. Reynolds, Hilal A. Lashuel, and Raffaele Mezzenga**

Abstract: *Tau protein and its fragments self-assemble into amyloid fibrils in the presence of polyanions, such as heparin. By combining microscopy, scattering, and spectroscopy techniques, we studied the aggregation of the 26-mer Tau-derived peptide alone, $Tau_{306–327}$, the third repeat fragment (R3) of the microtubule-binding domain. We show that: i) the sole $Tau_{306–327}$ can self-assemble into amyloid fibrils without the need of aggregation-promoting polyanions; ii) the resulting structures consist of surprisingly large, well-ordered 2D laminated flat ribbons, with a log-normal distribution of the lateral width, reaching the unprecedented lateral size of 350 nm and/or 45 individual protofilaments, that is, the largest amyloid laminated structures ever observed for Tau or any other amyloidogenic sequence. Our results provide insight into the molecular determinants of Tau aggregation and open new perspectives in the understanding of the assembly of amyloid fibrils and β-sheet-based biomaterials.*

The self-assembly of peptides and proteins, such as α-synuclein, Aβ peptide, and Tau protein, into β-sheet-rich fibrillar amyloid aggregates has been implicated in neurodegeneration and the pathogenesis of several devastating neurodegenerative disorders including Parkinson's and Alzheimer's diseases.[1,2] Advances in understanding the mechanism of amyloid formation has inspired the design of biomaterials with a wide-range of applications in medicine and biotechnology.[3]

Tau is a microtubule-binding protein and is the primary constituents of the neurofibrillary tangles found in the brain of Alzheimer's disease patients. Tau misfolding and aggregation is also thought to play a central role in the pathogenesis of several other human neurodegenerative diseases, known collectively as "tauopathies".[4] In vitro, the Tau protein does not aggregate spontaneously and adopts predominantly disordered conformations, but undergoes rapid aggregation in the presence of polyanions, such as heparin.[5]

Previous experimental studies have shown that the aggregation of Tau protein is strongly associated with two short amino acid sequences: one located in the third repeat fragment (R3, that is, VQIVYKPVDLSKVTSKCGSLGNIHHK) of the microtubule-binding domain of Tau, ^{306}VQIVYK^{311}, and its homologous sequence, ^{275}VQIINK^{280}, in the second repeat fragment. Both of these fragments have been shown to be critical in nucleating the self-assembly and formation of β-sheet-rich fibrillar aggregates of Tau.[6] The X-ray crystallographic structure of the sequence VQIVYK provided insight into the aggregation of Tau protein, showing paired layers of parallel, in-register β-sheets similar to those of many other amyloids.[7] Interestingly, the aggregation of the R3 fragment containing the ^{306}VQIVYK^{311} sequence, in the presence of heparin, leads to the formation of fibrillar structures that exhibit similar structural and morphological properties as those assembled from the full-length Tau protein.[8]

While investigating the self-assembly properties of the 26 amino acid peptide fragment that comprises the R3 domain of Tau ($Tau_{306-327}$), we observed that this peptide aggregates in the absence of heparin and forms giant, flat, multistranded amyloid ribbons generated from the lateral assembly of up to 45 individual protofilaments. This unparalleled lateral growth of protofilaments leads to an effective 2D laminated morphology, as confirmed by both atomic force microscopy (AFM) and small-angle X-ray scattering (SAXS), and suggests a potential role in artificial biomaterials design.

The occurrence of laminated ribbon structures has previously been observed during the self-assembly of several molecules, including a simple peptidomimetic,[9] the Aβ(16–22) peptide,[10] 20-mer peptides,[11] an amphiphilic dipeptide incorporated with an azobenzene moiety,[12] and hydrolyzed lysozyme and β-lactoglobulin proteins.[13] However, these laminated structures only reached a relatively low number of protofilaments, usually less than 20, maintaining the high aspect ratio typical of fibrous morphologies. Furthermore, and of more immediate significance, a lateral aggregation

[*] Dr. J. Adamcik, Dr. A. Sánchez-Ferrer, Prof. Dr. R. Mezzenga
Department of Health Sciences and Technology, ETH Zürich
Schmelzbergstrasse 9, LFO E23, 8092 Zürich (Switzerland)
E-mail: raffaele.mezzenga@hest.ethz.ch

N. Ait-Bouziad, Prof. Dr. H. A. Lashuel
Laboratory of Molecular and Chemical Biology of Neurodegeneration
Brain Mind Institute
Ecole Polytechnique Fédérale de Lausanne (EPFL)
1015 Lausanne (Switzerland)
and
Qatar Biomedical Research Institute
Hamad Bin Khalifa University
Doha, P.O. Box 5825 (Qatar)
E-mail: hilal.lashuel@epfl.ch

Dr. N. P. Reynolds
ARC Training Centre for Biodevices
Faculty of Science Engineering and Technology
Swinburne University of Technology
John Street, Melbourne, Vic 3122 (Australia)
and
Manufacturing Flagship, CSIRO
Bayview Avenue, Clayton, Vic 3169 (Australia)

Supporting information for this article is available on the WWW under http://dx.doi.org/10.1002/anie.201508968.

process leading to highly laminated structures has never been observed during the aggregation process of the Tau protein or fragments derived from it, neither in the presence nor absence of heparin.

Figure 1a shows the circular dichroism (CD) spectra of the R3 peptide incubated in buffer, in the absence of heparin,

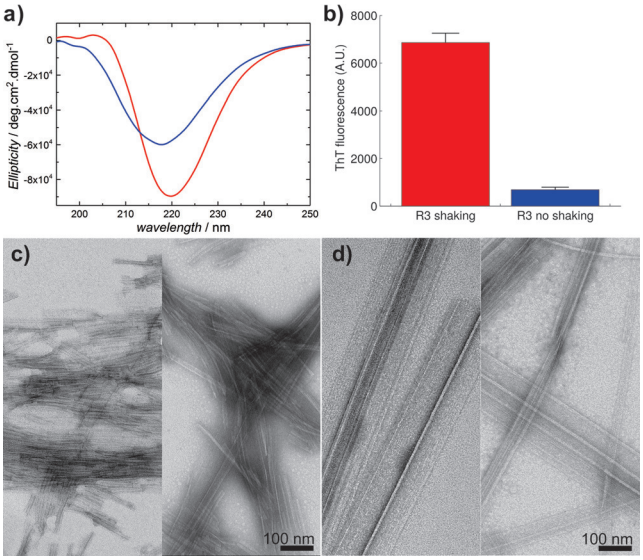

Figure 1. a) CD spectra of the R3 peptide incubated in buffer in the absence of heparin at 37 °C with shaking at 1000 rpm for 24 h (red color), and without shaking for 48 h (blue color). b) ThT fluorescence intensity of the peptide solutions incubated in buffer in the absence of heparin at 37 °C with either shaking at 1000 rpm for 24 h (red color), or without for 48 h (blue color). TEM images of self-assembled R3 peptide after incubation in buffer in the absence of heparin at 37 °C with shaking at 1000 rpm for 24 h (c), and without shaking for 48 h (d).

either with shaking at 1000 rpm or without shaking (under quiescent conditions). The spectra present a strong peak minimum at 220 nm and 218 nm, respectively, indicating the presence of β-sheet secondary structures, a typical hallmark of amyloid structures. Interestingly, when the R3 peptide was incubated in buffer containing heparin and with shaking at 1000 rpm for 24 h, the CD spectra also presents a peak minimum at 220 nm (Supporting Information, Figure S1a). To confirm if these β-sheet-rich ribbon-like structures possess amyloid-like properties, we assessed their ability to bind to the amyloid-specific dye Thioflavin T (ThT). Figure 1b shows that these structures bind to ThT, as evidenced by the increase in the fluorescence signal related to control or unaggregated peptide. The ThT fluorescence intensity of the R3 peptide solutions incubated in the absence of heparin, with or without shaking, is quite low in comparison to the intensity collected for the R3 peptide solution incubated in the presence of heparin with shaking (Figure S1b). These results indicate that the presence of heparin is not required for the formation of β-sheet secondary structure of R3 peptides, although it clearly enhances and accelerates the aggregation process. Under these conditions, transmission electron microscopy (TEM) images of the R3 peptide show a morphology reminiscent of amyloid structures, with rigid and flat ribbon-like morphologies with a wide distribution of widths (Figure 1c,d). Additional AFM and TEM images in the presence or absence of heparin revealed significantly different morphologies compared to the fibrillar structures (Supporting Information, Figures S2 and S3).[8]

All of these results confirm that the R3 peptide is capable of self-assembling into β-sheet-rich amyloid structures in the absence of heparin. Because the aggregation of R3 in the presence of heparin is already known[8] (see also Figure S2), we decided to focus next on conditions lacking heparin by using high-resolution AFM.

Figure 2 displays high-resolution AFM height images (Figure 2a,c) and the corresponding AFM phase images

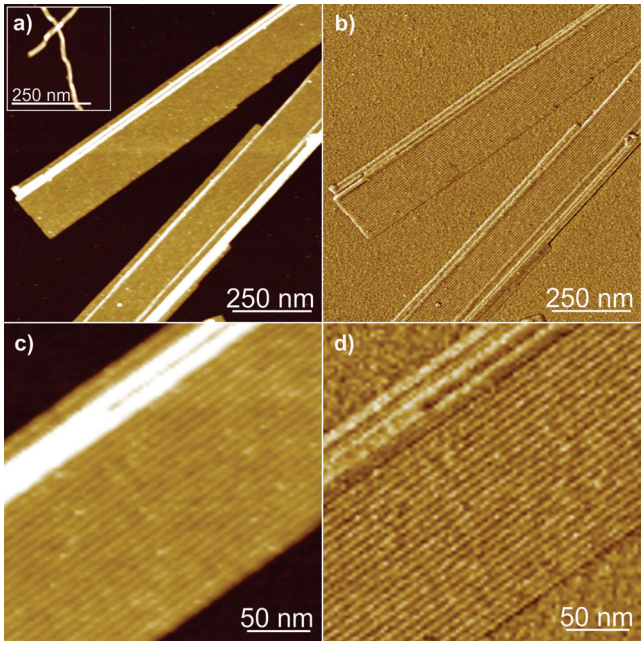

Figure 2. High-resolution AFM height images (a,c) with corresponding AFM phase images (b,d) of flat, multistranded ribbons self-assembled from the R3 peptide in the absence of heparin after incubation in buffer for 1 week at 37 °C without shaking. The inset in (a) displays, as a control, the fibrillar structure of the R3 peptide observed in the presence of heparin.

(Figure 2b,d) of the self-assembled R3 peptide after incubation for one week without heparin. Well-defined laminated, giant, flat ribbons containing many laterally assembled protofilaments in a 2D fashion are visible. In some cases, it is possible to observe other layers on top of the flat multistranded ribbons (Figure 2a,c). This contrasts sharply with the fibrillar structure observed for R3 in the presence of heparin (Figure 2a, inset). A representative gallery of AFM images is displayed in Figure S4. From the AFM images, the different thicknesses of the multistranded ribbons could be unambiguously resolved.

Figure 3 shows the analysis of the height measured for the multistranded ribbons. The lowest detectable maximum in height distributions of the ribbons was around 1.8 nm (Figure 3c).

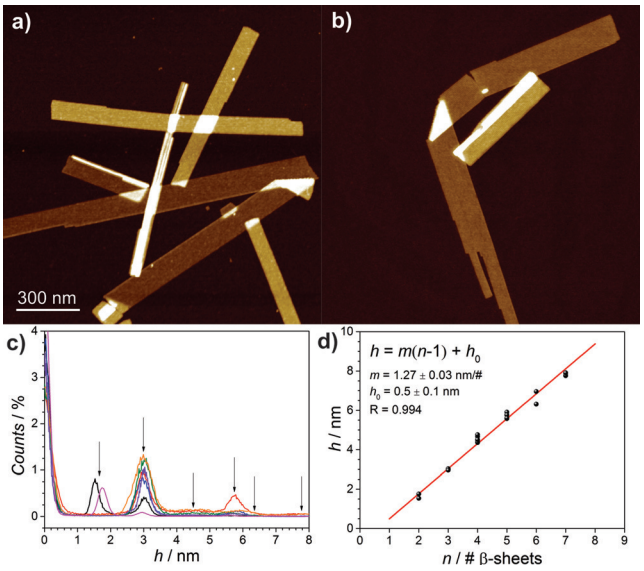

Figure 3. High-resolution AFM height images (a, b) of flat, multistranded ribbons self-assembled from the R3 peptide after incubation in buffer for 1 week at 37 °C in the absence of heparin, without shaking. c) The height distributions obtained from AFM images. Arrows indicate the maxima for different height distributions. d) Linear behavior between the height profile and the number of β-sheets in flat, multistranded ribbons. The minimum height is 1.27 ± 0.5 nm and the slope 1.27 ± 0.03 nm.

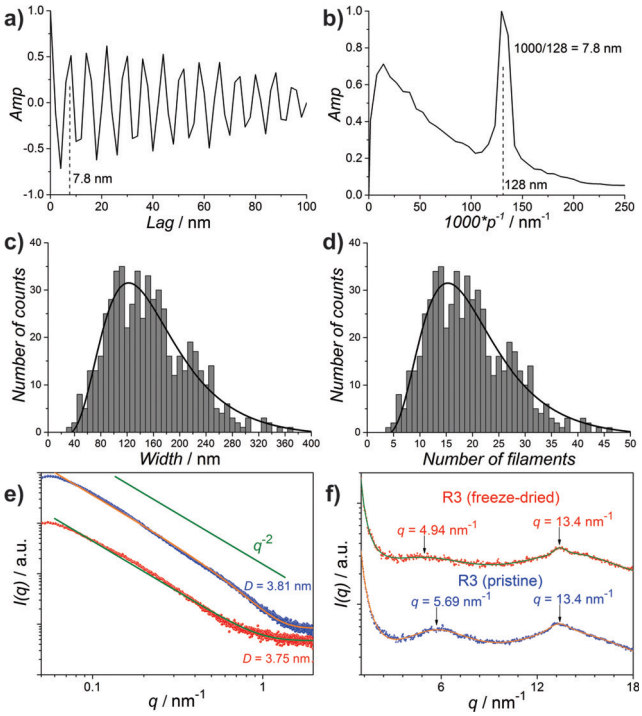

Figure 4. Determination of the distance between individual protofilaments within ribbons by: a) averaged autocorrelation functions of the transversal height profiles, and b) FFT analysis of the transversal height profiles perpendicular to the axis of flat, multistranded ribbons self-assembled from R3. Histogram of width distributions of flat multistranded ribbons self-assembled from the R3 peptide as a function of c) lateral width and d) number of aggregated lateral protofilaments. The continuous lines are log-normal fits, giving a mean value width of 149.7 nm and 18.7 protofilaments, respectively. e) SAXS intensity profile of 0.05 wt% (red color) and 1 wt% (blue color) dispersions of the R3 peptide. SAXS intensity profile in the low q-values region shows a q^{-2}-dependence, indicative of flat 2D particles, and the continuous lines are fits with the form factor of an infinitely large flat particle[16a] of thickness of 3.8 nm. f) WAXS intensity profile for the pristine (blue color) and freeze-dried (red color) R3 peptide.

Other maxima in height distributions showed values with approximately 1.3 nm of increase. The correlation of the maximum height with the number of β-sheets for different multistranded ribbons (Figure 3d) shows a good linear correlation ($R = 0.994$), with a slope of 1.27 ± 0.03 nm per β-sheet and an off-set of 0.5 ± 0.1 nm corresponding to the peptidic residues on both sides of the β-sheet.

To characterize the morphology of the multistranded ribbons in greater detail, the structural features were analyzed statistically using the open source code FiberApp.[14] Figure 4a and 4b show the distances between individual protofilaments in the multistranded ribbons extracted by two different methods: the height autocorrelation function and the Fast Fourier Transform (FFT) of the height signals, respectively. Based on the averaged autocorrelation functions (Figure 4a) and FFT (Figure 4b) of the transversal height profiles perpendicular to the axis of the multistranded ribbons, the distance between protofilaments was determined to be 7.8 nm. Thus, the constitutive protofilament of the highly laminated multistranded amyloid ribbons is resolved to have a pseudorectangular structure of 1.8 nm × 7.8 nm. The statistical distribution of the widths of the multistranded ribbons was also analyzed and the resulting histogram (Figure 4c) shows that the width of ribbons increases beyond 350 nm, following a log-normal distribution with a mean width value of 149.7 ± 4.2 nm. This unprecedented lateral size of 350 nm in laminated amyloid ribbons is much higher than any other laminated amyloid structure assembled. For example, the maximum reported sizes for comparable structures are 150 nm for peptidomimetics,[9] 130 nm for the Aβ(16–22) peptide,[10] 50 nm for 20 amino acid peptides,[11] 33 nm for amphiphilic dipeptide incorporated with an azobenzene moiety,[12] and 173 nm for hydrolyzed lysozyme and β-lactoglobulin.[13]

The lateral assembly histogram expressed in terms of number of protofilaments (Figure 4d) indicates that as many as 45 protofilaments assemble laterally to form the largest ribbons. To our knowledge, this is the largest number of protofilaments ever reported to co-assemble in the formation of a single individual amyloid fibril. The large number of protofilaments indicates the presence of very strong hydrophobic interactions, encoded by the sequence of the R3 fragment, that govern the lateral assembly of the constitutive protofilaments, analogous to other amyloid systems.[15]

The self-assembly of the R3 peptide in buffer without heparin at two different concentrations (low 0.05 wt% and high 1 wt%) was also analyzed by SAXS. Analysis of the SAXS intensity profiles for both concentrations (Figure 4e) revealed that at low scattering vector values (q) the slope of the spectra has a characteristic dependence on q^{-2}, indicative of a flat 2D morphology. A synchrotron SAXS kinetic study over different incubation times confirmed that this q^{-2}-

dependence was already evident after 24 h (Figure S5). Similar q^{-2} slopes have also been identified for flat 2D particles, owing to the assembly of the ILQINS hexapetide[16a] or arginine-coated peptide,[16b] strongly suggesting similar assembly for the R3 peptide. Thus, the SAXS results independently confirm the highly laminated structures observed for R3 by microscopy.

Wide-angle X-ray scattering (WAXS) experiments were also performed on the pristine powder, as well as the freeze-dried powder obtained from the 1 wt% dispersion (Figure 4 f). The results show the presence of two peaks for both powder samples. The inter-β-sheet distance at $q = 5.7$ (pristine sample) and 4.9 (freeze-dried sample) nm^{-1}, and the inter-β-strand distance at $q = 13.4\ nm^{-1}$. The first peak corresponds to a distance of 1.10 and 1.27 nm for the pristine and the freeze-dried sample, respectively, with very low correlation lengths of approximately $\xi = 1$ nm. This distance is in agreement with the slope of 1.27 nm obtained from the AFM analysis, and the low correlation length value indicates the low statistical number of β-sheets per multistranded ribbon. The second peak at high q-value corresponds to the typical distance of 0.47 nm characteristic of the interspacing among β-strands typically found in amyloid structures, with correlation lengths from 4 to 7 nm. The WAXS analysis corroborates both the CD spectroscopy and ThT fluorescence experiments in resolving the typical secondary structure of amyloid fibrils in R3 aggregation.

By combining the structural features from the AFM analysis with the amyloid fingerprint revealed by CD, ThT, and WAXS, a molecular packing of the R3 peptide within the constitutive 1.8 nm × 7.8 nm protofilament can be proposed. By taking the average length of a peptidic bond as 3.6 Å, the fully extended R3 26-mer should have a length of 9.4 nm. Molecular modelling of the peptide sequence (semi-empirical quantum mechanics method) gave an end-to-end distance of 8.3 nm, with a kink in the β-strand owing to the presence of a proline residue in the 7th amino acid, consistent with the 7.8 nm measured by AFM. Figure 5 shows a proposed structural model of the R3 peptide self-assembly and protofilament formation based on all of the measurements reported here, which is consistent with modeling results.[17]

In summary, we used the microscopy techniques TEM and AFM, in combination with CD spectroscopy, ThT fluorescence, and X-ray scattering, to investigate and characterize the self-assembly of the R3 26-mer, $Tau_{306-327}$, comprising the third repeat fragment of the microtubule-binding domain of the Tau protein. While the R3 peptide in the presence of heparin self-assembles into typical fibrillar amyloid structures[8] (see also inset of Figure 2 a and Figure S2), R3 self-assembles in the absence of heparin into large, flat, multistranded ribbons consisting of up to 45 laterally assembled protofilaments. These results indicate that the Tau protein and fragments derived from it, such as the R3 peptide, may assemble into amyloid structures of surprising dimensions in the absence of aggregation-enhancing species, such as heparin or alternative polyanions. These results may open new perspectives on the potential roles of hydrophobic interactions in guiding the lateral 2D assembly of amyloid proteins that are the defining hallmarks of neurodegenerative diseases. In particular, the presence of directional interactions among protofilaments can be be inferred from the 2D structures, analogous to patchy-like hydrophobic interactions.[15] Finally, our results may have implications on ex-novo design of β-sheet-based materials for biomaterials, scaffolding, templating, and nanotechnology applications.

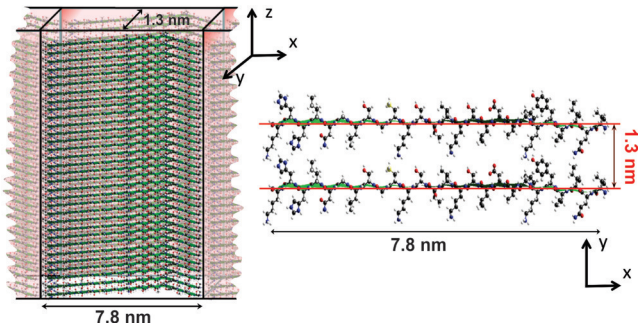

Figure 5. Illustration showing the self-assembly of R3 peptide into protofilaments of 7.8 nm thickness. The distance between two β-sheets is 1.3 nm with an off-set of ca 0.4–0.6 nm corresponding to the peptidic residues at both sides of the β-sheet.

Keywords: AFM · amyloids · peptide ribbons · self-assembly · statistical analysis

How to cite: *Angew. Chem. Int. Ed.* **2016**, *55*, 618–622
Angew. Chem. **2016**, *128*, 628–632

[1] E. M. Mandelkow, E. Mandelkow, *Cold Spring Harbor Perspect. Med.* **2012**, *2*, a006247.
[2] a) F. Chiti, C. M. Dobson, *Annu. Rev. Biochem.* **2006**, *75*, 333–366; b) P. K. Auluck, G. Caraveo, S. Lindquist, *Annu. Rev. Cell Dev. Biol.* **2010**, *26*, 211–233; c) C. L. Masters, D. J. Selkoe, *Cold Spring Harbor Perspect. Med.* **2012**, *2*, a006262; d) I. W. Hamley, *Chem. Rev.* **2012**, *112*, 5147–5192.
[3] a) S. Zhang, *Nat. Biotechnol.* **2003**, *21*, 1171–1178; b) E. Gazit, *Chem. Soc. Rev.* **2007**, *36*, 1263–1269.
[4] a) C. Ballatore, V. M. Lee, J. Q. Trojanowski, *Nat. Rev. Neurosci.* **2007**, *8*, 663–672; b) M. G. Spillantini, M. Goedert, *Lancet Neurol.* **2013**, *12*, 609–622.
[5] a) M. Goedert, R. Jakes, M. G. Spillantini, M. Hasegawa, M. J. Smith, R. A. Crowther, *Nature* **1996**, *383*, 550–553; b) N. Sibille, A. Sillen, A. Leroy, J. M. Wieruszeski, B. Mulloy, I. Landrieu, G. Lippens, *Biochemistry* **2006**, *45*, 12560–12572; c) S. Jeganathan, M. von Bergen, E. M. Mandelkow, E. Mandelkow, *Biochemistry* **2008**, *47*, 10526–10539; d) H. L. Zhu, C. Fernández, J. B. Fan, F. Shewmaker, J. Chen, A. P. Minton, Y. Liang, *J. Biol. Chem.* **2010**, *285*, 3592–3599.
[6] a) M. von Bergen, P. Friedhoff, J. Biernat, J. Heberle, E. M. Mandelkow, E. Mandelkow, *Proc. Natl. Acad. Sci. USA* **2000**, *97*, 5129–5134; b) W. Li, V. M. Lee, *Biochemistry* **2006**, *45*, 15692–15701; c) E. Mandelkow, M. von Bergen, J. Biernat, E. M. Mandelkow, *Brain Pathol.* **2007**, *17*, 83–90; d) P. Ganguly, T. D. Do, L. Larini, N. E. LaPointe, A. J. Sercel, M. F. Shade, S. C. Feinstein, M. T. Bowers, J. E. Shea, *J. Phys. Chem. B* **2015**, *119*, 4582–4593.
[7] a) M. R. Sawaya, S. Sambashivan, R. Nelson, M. I. Ivanova, S. A. Sievers, M. I. Apostol, M. J. Thompson, M. Balbirnie, J. J. Wiltzius, H. T. McFarlane, A. O. Madsen, C. Riekel, D. Eisenberg, *Nature* **2007**, *447*, 453–457; b) V. Daebel, S. Chinnathambi, J. Biernat, M. Schwalbe, B. Habenstein, A. Loquet, E. Akoury, K. Tepper, H. Müller, M. Baldus, C. Griesinger, M. Zweckstet-

ter, E. Mandelkow, V. Vijayan, A. Lange, *J. Am. Chem. Soc.* **2012**, *134*, 13982 – 13989.
[8] K. Minoura, T. M. Yao, K. Tomoo, M. Sumida, M. Sasaki, T. Taniguchi, T. Ishida, *Eur. J. Biochem.* **2004**, *271*, 545 – 552.
[9] H. A. Lashuel, S. R. Labrenz, L. Woo, L. C. Serpell, J. W. Kelly, *J. Am. Chem. Soc.* **2000**, *122*, 5262 – 5277.
[10] K. Lu, J. Jacob, P. Thiyagarajan, V. P. Conticello, D. G. Lynn, *J. Am. Chem. Soc.* **2003**, *125*, 6391 – 6393.
[11] a) M. S. Lamm, K. Rajagopal, J. P. Schneider, D. J. Pochan, *J. Am. Chem. Soc.* **2005**, *127*, 16692 – 16700; b) R. A. Hule, R. P. Nagarkar, B. Hammouda, J. P. Schneider, D. J. Pochan, *Macromolecules* **2009**, *42*, 7137 – 7145.
[12] Y. Y. Lin, Y. Qiao, P. F. Tang, Z. B. Li, J. B. Huang, *Soft Matter* **2011**, *7*, 2762 – 2769.
[13] C. Lara, J. Adamcik, S. Jordens, R. Mezzenga, *Biomacromolecules* **2011**, *12*, 1868 – 1875.
[14] I. Usov, R. Mezzenga, *Macromolecules* **2015**, *48*, 1269 – 1280.
[15] a) J. Adamcik, J.-M. Jung, J. Flakowski, P. De Los Rios, G. Dietler, R. Mezzenga, *Nat. Nanotechnol.* **2010**, *5*, 423 – 428; b) R. Mezzenga, P. Fischer, *Rep. Prog. Phys.* **2013**, *76*, 046601.
[16] a) C. Lara, N. P. Reynolds, J. T. Berryman, A. Xu, A. Zhang, R. Mezzenga, *J. Am. Chem. Soc.* **2014**, *136*, 4732 – 4739; b) I. W. Hamley, A. Dehsorkhi, V. Castelletto, *Chem. Commun.* **2013**, *49*, 1850 – 1852.
[17] A. Siddiqua, Y. Luo, V. Meyer, M. A. Swanson, X. Yu, G. Wei, J. Zheng, G. R. Eaton, B. Ma, R. Nussinov, S. S. Eaton, M. Margittai, *J. Am. Chem. Soc.* **2012**, *134*, 10271 – 10278.

Received: September 25, 2015
Revised: November 7, 2015
Published online: December 7, 2015

